Synthesis and Characterization of a Series of Zinc Bis[(alkyl)(trimethylsilyl)amide] Compounds

David A. Gaul,[†,§] Oliver Just,[†,§] and William S. Rees, Jr.*[,†,‡,§]

School of Chemistry and Biochemistry, School of Materials Science and Engineering, and Molecular Design Institute, Georgia Institute of Technology, Atlanta, Georgia 30332-0400

Received March 2, 2000

A series of 21 secondary (alkyl)(trimethylsilyl)amines HNR(TMS) [R = *n*-propyl (**1**), *i*-propyl (**2**), *n*-butyl (**3**), *i*-butyl (**4**), *s*-butyl (**5**), *tert*-butyl (**6**), *c*-pentyl (**7**), *n*-pentyl (**8**), *i*-pentyl (**9**), 1-methylbutyl (**10**), 2-methylbutyl (**11**), 1-ethylpropyl (**12**), 1,2-dimethylpropyl (**13**), *tert*-pentyl (**14**), phenyl (**15**), *c*-hexyl (**16**), *n*-hexyl (**17**), *N*,*N*-dimethyl-3-aminopropyl (**18**), benzyl (**19**), *n*-heptyl (**20**), 1,1,3,3-*tert*-butyl (**21**); TMS = $Si(CH_3)_3$] has been prepared and fully characterized by elemental analyses, multinuclear (^1H, ^{13}C, ^{29}Si, ^{14}N) NMR, IR, UV/vis, MS, and boiling point. A new method for determination of boiling points of milligram-size samples, based on DSC (differential scanning calorimetry), is described. Each amine has been converted to the corresponding zinc bis(amide) compound $Zn[N(TMS)(R)]_2$ [R = *n*-propyl (**22**), *i*-propyl (**23**), *n*-butyl (**24**), *i*-butyl (**25**), *s*-butyl (**26**), *tert*-butyl (**27**), *c*-pentyl (**28**), *n*-pentyl (**29**), *i*-pentyl (**30**), 1-methylbutyl (**31**), 2-methylbutyl (**32**), 1-ethylpropyl (**33**), 1,2-dimethylpropyl (**34**), *tert*-pentyl (**35**), phenyl (**36**), *c*-hexyl (**37**), *n*-hexyl (**38**), *N*,*N*-dimethyl-3-aminopropyl (**39**), benzyl (**40**), *n*-heptyl (**41**), 1,1,3,3-*tert*-butyl (**42**); TMS = $Si(CH_3)_3$] and subsequently fully characterized by elemental analyses, multinuclear (^1H, ^{13}C, ^{29}Si, ^{14}N) NMR, IR, UV/vis, MS, and TGA. The experimental IR has been compared to the computationally calculated one for compound **27**. Observed trends in volatility of the compounds are discussed in the context of the dominant intermolecular forces present in the condensed phase.

Introduction

Zinc selenide presently is one potential lead candidate for solid-state inorganic optoelectronic devices operating in the blue region of the visible spectrum.[1−6] The current bottleneck in this materials system is achievement of a reproducible, highly active p-type composition.[7] One route to address this fundamental issue is to deliver a high flux of nitrogen dopant atoms to the electronically active (selenium) sublattice residence. A potential solution is to design a precursor that links the dopant nitrogen to the zinc. Thus, in the instances when a Zn−N bond of a precursor molecule is retained throughout the decomposition process, the nitrogen atom has an enforced residence on a lattice site adjacent to a native zinc location, a consequence of the lack of an appreciable zinc antisite defect density in this semiconductor material. Previously, compounds of the general formula (R)(R′)NZnN(R″)(R‴) (Figure 1) have demonstrated the potential to retain a zinc−nitrogen interaction during the thermal decomposition process.[8−13] As a consequence of these promising results, a detailed systematic approach was developed

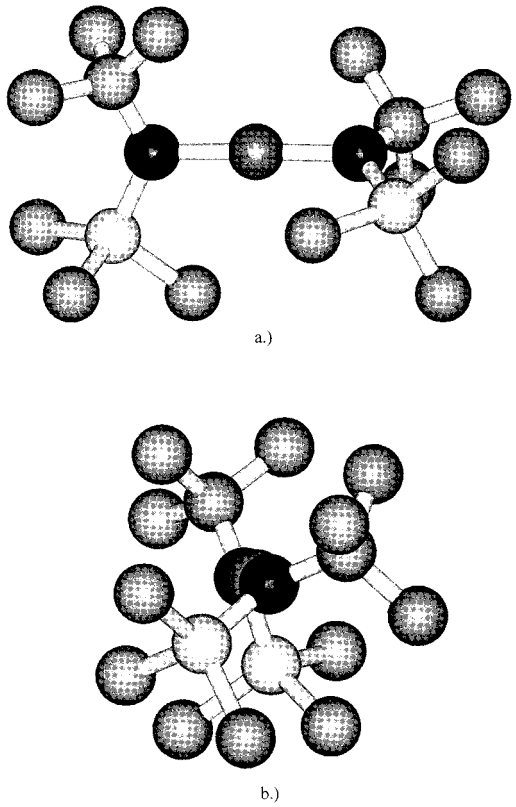

Figure 1. General structure of $Zn[N(tert\text{-butyl})(Si(CH_3)_3)]_2$: (a) view perpendicular to the N−Zn−N axis; (b) view along the N−Zn−N axis.

* To whom correspondence should be addressed. Phone: 404-894-4049. Fax: 404-894-1144. E-Mail: will.rees@chemistry.gatech.edu.
† School of Chemistry and Biochemistry.
‡ School of Materials Science and Engineering.
§ Molecular Design Institute.

(1) Nakanishi, K.; Suemune, I.; Kuroda, Y.; Yamanishi, M. *Appl. Phys. Lett*. **1991**, *59*, 1401.
(2) Zmudzinski, C.; Guan, Y.; Zory, P. *IEEE Photon. Technol. Lett*. **1990**, *2*, 94.
(3) Haase, M.; Qiv, J.; DePuydt, J.; Cheng, H. *Appl. Phys. Lett*. **1991**, *59*, 1272.
(4) Qiv, J.; DePuydt, J.; Cheng, H.; Haase, M. *Appl. Phys. Lett.* **1991**, *59*, 1992.
(5) Haase, M.; Cheng, H.; Misemer, D.; Strand, T.; DePuydt, J. *Appl. Phys. Lett*. **1991**, *59*, 3619.
(6) Jeon, H.; Ding, J.; Patterson, W.; Nurmikiko, A.; Xie, W.; Grilla, D.; Kobayashi, M.; Gunshor, R. *Appl. Phys. Lett*. **1991**, *59*, 3619.
(7) (a) Matsuoka, T. *Adv. Mater*. **1996**, *8*, 469. (b) Rees, W. S., Jr.; Gaul, D. A. *Adv. Mater.* **2000**, *12*, 935.

10.1021/ic000234j CCC: $19.00
Published on Web 11/10/2000

to probe the effects of ligand manipulation on the vapor-phase stability, as well as the vapor pressure. In the search for an optimized precursor, the focus is directed toward maximizing volatility while minimizing ligand girth required to protect the metal center. A series of bis[(alkyl)(trimethylsilyl)amide] compounds of zinc has been prepared and characterized by a variety of techniques. These results are reported herein.

Experimental Section

General Information. All gases (Air Products, Holox) were of high (99.999%) purity and used following purification with activated Ridox catalyst and Sicapent to remove traces of oxygen and moisture, respectively. All solvents were reagent grade, available from commercial suppliers, and purified according to standard literature techniques.[14] All the primary amines (Aldrich Chemical Co.) were analyzed by GC/MS, ^{1}H NMR, and ^{13}C NMR and used as received except aniline (Aldrich Chemical Co.), which was distilled from KOH prior to usage. Trimethylchlorosilane (Aldrich Chemical Co., Gelest) was analyzed by ^{1}H NMR and used as received. *n*-Butyllithium (10 M) in hexane (Aldrich Chemical Co.) was diluted to between 2 and 3 M and then titrated with standardized 1 M hydrochloric acid according to the Gilman double titration protocol.[15] Anhydrous zinc dichloride (Strem) was used as received. Deuterated benzene and toluene (Cambridge Isotope Laboratories, Inc.) were distilled from sodium and stored in an inert atmosphere glovebox. Deuterated water (Aldrich Chemical Co.) was used as received. All sample preparations involving air- and moisture-sensitive products were performed in an inert atmosphere glovebox (VAC MO-40-M-SSG).

^{1}H NMR (300 MHz), ^{13}C{^{1}H} NMR (75.432 MHz), ^{29}Si NMR (59.595 MHz), and ^{14}N NMR (21.611 MHz) spectra were recorded on either a Varian Gemini-300 or a Bruker AMX 400 spectrometer. Chemical shifts are reported in ppm on a $+\delta$ scale upfield with resonances from the NMR solvents serving as internal standards for the ^{1}H (residual C_6HD_5 in C_6D_6, $\delta = 7.15$ ppm, or residual $C_6H_5CHD_2$ in $C_6D_5CD_3$, $\delta = 2.09$ ppm) and ^{13}C (C_6D_6, $\delta = 128.0$ ppm) spectra. External standards were employed for ^{29}Si ($Si(CH_3)_4$ in C_6D_6, $\delta = 0$ ppm) and ^{14}N (NH_4NO_3 in D_2O, $\delta = 0$ ppm) spectra. Variable temperature spectra for $Zn[N(n\text{-propyl})(Si(CH_3)_3)]_2$ were obtained on a Bruker AMX 400 spectrometer. All samples were dissolved in C_6D_6, except for **22** when deuterated toluene was used, and vacuum-sealed. Temperature calibration of the spectrometers was accomplished by observing ethylene glycol for temperatures above ambient while methanol was employed for the subambient temperatures.[16,17]

Gas chromatogram/mass spectra for the secondary alkylsilylamines were obtained with a Hewlett-Packard 5890 series II plus GC equipped with a split-flow injected, 30 m × 0.25 mm, cross-linked, 5% methylphenylsiloxane capillary column interfaced to a Hewlett-Packard MS 5972 series mass spectrometer under a He gas flow with a 70 eV EI ion source and are reported as m/e^+. The low-resolution mass spectra for the zinc bis(amide) compounds were collected using a VG Instruments 70SE spectrometer with a 70 eV EI ion source, in a vacuum of 10^{-6} Torr, employing a direct insertion probe. The samples were flame-sealed in melting point capillaries at ambient pressure and broken open immediately prior to insertion into the spectrometer. Once inserted, the sample was heated at a rate of 2 °C/s.

IR spectra of neat liquids were obtained using either KBr or CsI plates either on a Nicolet 520 FT-IR (4000−400 cm^{-1}) or on a Nicolet 60SXR FT-IR (500−200 cm^{-1}) equipped with a glowbar, 6 μm Mylar beam splitter, and a TGS detector and are reported in cm^{-1}. Solid samples were prepared as Nujol mulls. UV/vis spectra were taken as THF solutions (vs THF) in 1 cm quartz cells with Teflon caps on a Perkin-Elmer UV/vis/NIR Lambda 19 spectrophotometer and are reported in nanometers.

Elemental analyses for carbon and hydrogen content were measured in sealed volatile sample pans using a Perkin-Elmer series II CHNS/O 2400 analyzer. Zinc content was determined using a Perkin-Elmer OPTIMA 3000 ICP-OES analyzer. Solutions of zinc dichloride dissolved in ca. 15% nitric acid ranging from 0.0001 to 10 ppm were used to calibrate the instrument. Zinc bis(amide) compounds dissolved in ca. 15% nitric acid were prepared with an approximate zinc concentration of 1 ppm.

Differential scanning calorimetry (DSC) data for secondary amines were collected in aluminum sample pans with 50 μm laser-drilled holes in the lids using a Perkin-Elmer DSC 7 with an Ar purge of 15 sccm. Samples were prepared by measuring 7 μL of the amine, employing a 10 μL glass syringe, into the sample pan, which then was sealed by crimping in a mechanical press. Following an initial equilibrium time of 1 min, a heating rate of 10 °C/min was selected to collect the endotherms. Thermogravimetric analyses were recorded on a Perkin-Elmer TGA7 inside an inert atmosphere glovebox. Between 5 and 20 mg of each compound was loaded into a platinum sample pan and placed into the furnace with an Ar purge rate of 15 sccm. A temperature program consisting of a heating rate of 10 °C/min was used to collect the thermograms. Melting points were obtained in capillaries sealed with silicon grease using a Laboratory Devices MEL-TEMP II, and boiling points were measured during product purification (Table 16 of Supporting Information).

Molecular modeling was performed using a Silicon Graphics Indigo-2 data station incorporating BIOSYM software, specifically the Discover3 (ESFF force field), MOPAC (AM1), and Turbomole (Hartree−Fock) modules.

Preparations. All reactions were performed under a positive pressure of Ar in oven-dried glassware using predried, degassed solvents. All oxygen- and moisture-sensitive products were stored and handled in an inert atmosphere glovebox.

1. Method A for Synthesis of (Alkyl)(trimethylsilyl)amines. Two equivalents of a primary amine were dissolved in 500 mL of diethyl ether and placed in a three-necked, round-bottomed 1 L flask equipped with a Teflon-coated metallic stir bar, septum, gas inlet, and a stopper. One equivalent of trimethylchlorosilane was added dropwise to the vigorously stirred solution at 0 °C, resulting in an instantaneous precipitation of a voluminous white solid. Upon completion of the addition, the reaction mixture was allowed to attain ambient temperature on its own and was left to stir for an additional 2 h. In ensuing Schlenk filtration, the hydrochloride salt of the corresponding amine was separated and subsequently washed several times with small portions of diethyl ether to maximize the yield. After the solvent was removed at ambient pressure, each amine was isolated by distillation as a colorless liquid. Compound characterizations are reported in Tables 1−8 in the Supporting Information.

2. Method B for Synthesis of (Alkyl)(trimethylsilyl)amines. A primary amine dissolved in 100 mL of diethyl ether was placed in a three-necked round-bottomed 500 mL flask equipped with a Teflon coated metallic stir bar, septum, gas inlet, and a stopper. At ambient temperature, a stoichiometric amount of *n*-BuLi was added dropwise under vigorous stirring, resulting, except for **22**, in a precipitation of a white solid. After the mixture was stirred overnight, 1 equiv of trimethylchlorosilane was added dropwise at ambient temperature. The reaction mixture was then left to stir for another 12 h, and the lithium chloride was subsequently separated by Schlenk filtration. In analogy to method A, each amine was isolated by distillation as a colorless liquid.

(8) Rees, W. S., Jr.; Anderson, T.; Green, D.; Bretschneider, E. *Wide Band-Gap Semiconductors*; Moustakes, T., Pankove, J., Hamakawa, Y., Eds.; *Mater. Res. Soc. Proc*. **1992**, *242*, 281.
(9) Rees, W. S., Jr.; Green, D.; Anderson, T.; Bretschneider, E.; Pathangey, B.; Kim, J. *J. Electron. Mater.* **1992**, *21*, 361.
(10) Rees, W. S., Jr.; Green, D.; Hesse, W.; Anderson, T.; Pathangey, B. Chemical Perspectives of Microelectronic Materials. *Mater. Res. Soc. Proc*. **1992**, *282*, 63.
(11) Rees, W. S., Jr.; Green, D.; Hesse, W. *Polyhedron* **1992**, *11*, 1667.
(12) Rees, W. S., Jr.; Just, O. Gas-Phase and Surface Chemistry in Electronic Materials Processing. *Mater. Res. Soc. Proc*. **1994**, *334*, 219.
(13) Gaul, D.; Just, O.; Rees, W. S., Jr. Metal-Organic Chemical Vapor Deposition of Electronic Ceramics II. *Mater. Res. Soc. Proc*. **1996**, *415*, 117.
(14) Perrin, D.; Armarego, W. *Purification of Laboratory Chemicals*, 3rd ed.; Pergamon Press: New York, 1988.
(15) Gilman, H.; Cartledge, F. *J. Organomet. Chem*. **1964**, *2*, 447.
(16) Van Geet, A. *Anal. Chem*. **1968**, *40*, 22.
(17) Van Geet, A. *Anal. Chem*. **1970**, *42*, 679.

Scheme 1. General Synthetic Route for HN(R)(TMS)[a]

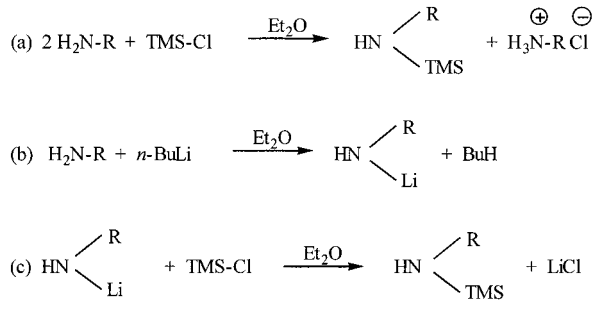

[a] R = *n*-propyl (**1**), *i*-propyl (**2**), *n*-butyl (**3**); *i*-butyl (**4**), *s*-butyl (**5**), *tert*-butyl (**6**), *c*-pentyl (**7**), *n*-pentyl (**8**), *i*-pentyl (**9**), 1-methylbutyl (**10**), 2-methylbutyl (**11**), 1-ethylpropyl (**12**), 1,2-dimethylpropyl (**13**), *tert*-pentyl (**14**), phenyl (**15**), *c*-hexyl (**16**), *n*-hexyl (**17**), *N*,*N*-dimethyl-3-aminopropyl (**18**), benzyl (**19**), *n*-heptyl (**20**), 1,1,3,3-*tert*-butyl (**21**); TMS = $Si(CH_3)_3$.

3. Synthesis of Zinc Bis(amide) Compounds. A 100 mL Schlenk flask containing a Teflon coated metallic stir bar and a septum was charged with a secondary amine dissolved in 50 mL of diethyl ether. A stoichiometric amount of *n*-BuLi was added dropwise under vigorous stirring at ambient temperature, and the reaction mixture was left to stir for 12 h. Subsequently, it was added via a cannula in a 2:1 molar ratio to a vigorously stirred zinc dichloride/diethyl ether solution (50 mL) at 0 °C. The lithium chloride precipitate was separated by Schlenk filtration, and all volatiles were removed under reduced pressure. All zinc amides, which are colorless liquids or solids under ambient conditions, were isolated and purified by methods given in Table 16 of the Supporting Information. The characterization data are given in Tables 9−16 of the Supporting Information.

Results

1. Preparation. Secondary Amines. Syntheses of the secondary (alkyl)(trimethylsilyl)amine compounds utilized in the present study were accomplished by employment of either of two routes (Scheme 1). All reactions were performed under an atmosphere of argon. The first method involves addition of trimethylchlorosilane to 2 equiv of a primary amine in diethyl ether (Scheme 1a).[18] Formation of the desired (alkyl)(trimethylsilyl)amine was accompanied by an instantaneous precipitation of quaternary ammonium chloride. To enhance conversion of the primary amine, an alternative route was pursued for selected secondary amines.

The alternative method involves metalation of a primary amine with *n*-butyllithium (Scheme 1b). With the exception of compound **21**, all of the investigated lithium amides were insoluble in the reaction medium. The next step consisted of reacting the lithium amide with trimethylchlorosilane (Scheme 1c).[11] Isolated yields in this two-step, one-pot reaction consistently were higher than those observed for the first method (Table 7 of the Supporting Information).

2. Purification. The amine hydrochloride salt (Scheme 1a) or the lithium chloride precipitate (Scheme 1b) was removed either by Schlenk filtration or by decantation of the clear solution. For the lower boiling compounds (<150 °C), the products were isolated by distillation at ambient pressure as colorless liquids. For the higher boiling derivatives, the solvents first were removed under reduced pressure and subsequently the products were vacuum-distilled to yield colorless liquids. All synthesized compounds are stable species under an inert gas atmosphere under ambient conditions.

3. Spectroscopic Properties. A. ^{1}H, ^{13}C, ^{29}Si, and ^{14}N NMR. The observed NMR spectra for each nucleus correlated well with the expected chemical shifts for each of the compounds. In the ^{1}H spectrum, the amine proton peak (when observed) was a broad (∼24 Hz width at half-height) singlet. The quadrupolar ^{14}N nucleus produced broadened signals with an average width at half-height of about 20 ppm. The NMR data are compiled in Tables 1−3 in the Supporting Information.

B. MS. The molecular ion peak and the next four major mass peaks for each secondary amine are reported in Table 4 in the Supporting Information.

C. IR. Twenty-four of the most intense peaks within the range 4000−200 cm^{-1} for each secondary amine are catalogued in Table 5 in the Supporting Information.

D. UV/Vis. Observed λ maxima from the UV/vis spectra are shown in Table 6 of the Supporting Information for each secondary amine. Molar absorptivities, calculated from Beer's law, are also listed.

4. Elemental Composition. C/H Elemental Analysis. The bulk purity of all (alkyl)(trimethylsilyl)amine derivatives was verified by determining their carbon and hydrogen content. The theoretical and the experimental values for these analyses are contained in Table 7 of the Supporting Information.

5. Thermal Properties. DSC. Boiling points at atmospheric pressure for each of the secondary amines were determined utilizing DSC, by calculating the onset of the endothermic event. Observed values correlated well with literature data for known species. The results are listed in Table 8 of the Supporting Information.

Scheme 2. General Synthetic Route for Zn[N(R)(TMS)]$_2$[a]

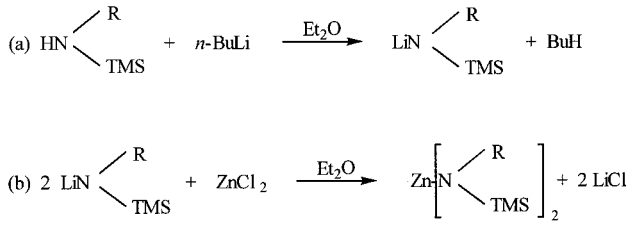

[a] R = *n*-propyl (**22**), *i*-propyl (**23**), *n*-butyl (**24**), *i*-butyl (**25**), *s*-butyl (**26**), *tert*-butyl (**27**), *c*-pentyl (**28**), *n*-pentyl (**29**), *i*-pentyl (**30**), 1-methylbutyl (**31**), 2-methylbutyl (**32**), 1-ethylpropyl (**33**), 1,2-dimethylpropyl (**34**), *tert*-pentyl (**35**), phenyl (**36**), *c*-hexyl (**37**), *n*-hexyl (**38**), *N*,*N*-dimethyl-3-aminopropyl (**39**), benzyl (**40**), *n*-heptyl (**41**), 1,1,3,3-*tert*-butyl (**42**); TMS = $Si(CH_3)_3$.

1. Preparation. Zinc Bis(Amide) Compounds. All zinc bis[alkyl(trimethylsilyl)amide] compounds **22**−**42** (Table 14 of the Supporting Information) were synthesized according to Scheme 2.[11,19,20] Each reaction was performed under an argon atmosphere. The first step in this sequence is comprised of the metalation of the secondary amine with *n*-butyllithium. In a 2:1 ratio, the lithiated amine was subsequently added to a solution of zinc dichloride at 0 °C. During the addition, lithium chloride precipitates as a white solid.

2. Purification. Lithium chloride was removed either by Schlenk filtration or by decanting the clear solution. The solvent was removed under reduced pressure. The product was isolated by vapor transfer, distillation, recrystallization at subambient temperature, or any combination thereof to yield colorless liquids or solids. The isolated yields of purified bulk compounds are listed in Table 15 of the Supporting Information for the zinc bis(amide) compounds.[21] The boiling and the melting points

(18) Courtois, G.; Miginiac, L. *Tetrahedron Lett*. **1987**, *28*, 1659.

(19) Burger, H.; Sawodny, W.; Wannagat, U. *J. Organomet. Chem*. **1965**, *3*, 113.

(20) Power, P.; Ruhlandt-Senge, K.; Shoner, S. *Inorg. Chem*. **1991**, *30*, 5013.

(21) Only compound **41** is reported as unpurified yield.

(for ambient condition solid compositions) are collected in Table 16 of the Supporting Information.

3. Spectroscopic Characterization. A. ^{1}H NMR. The spectra of the zinc bis(amide) compounds agreed with anticipated results, except for compounds **22**, **24**, **29**, **30**, **38**, and **41**, when two sets of peaks were observed at ambient temperature. Elevated-temperature experiments (353 K) for each of these species resulted in peak coalescence. For compounds **36** and **40** only data at 353 K were obtained. The results are listed in Table 9 of the Supporting Information. Variable temperature experiments were performed using a 400 MHz NMR spectrometer to investigate the dynamic processes involved. Figure 5 of the Supporting Information displays the region associated with the protons of the trimethylsilyl substituent for compound **22** (toluene-d_8 solution).

B. ^{13}C NMR. Similar to the ^{1}H data, the observed resonances for **22**, **24**, **29**, **30**, **38**, and **41** consisted of two sets at ambient temperature. Peak coalescence was observed at 353 K. For compounds **36** and **40** only data at 353 K were obtained. In addition, the chiral ligands **5**, **10**, **11**, and **13** yielded multiple isomeric forms of the corresponding zinc bis(amide) compounds **26**, **31**, **32**, and **34**. The data are tabulated in Table 10 of the Supporting Information.

C. ^{29}Si and ^{14}N NMR. Ambient temperature ^{29}Si shifts for **22**, **24**, **29**, **30**, **38**, and **41** were split into two signals. Experiments at 353 K resulted in broadened resonances (~160 Hz width at half-height). Additionally, compounds **36** and **40** displayed multiple environments at ambient temperature; however, the elevated-temperature experiments resulted in peak coalescence. The data are listed in Table 11 of the Supporting Information, along with the ^{14}N data, whose shifts and appearance quantitatively were similar to those observed for the corresponding secondary amines.

D. MS. Results of the molecular ions and the next four most prominent peaks from the EI-MS are compiled in Table 12 of the Supporting Information. Zinc-containing species have a characteristic isotopic pattern, which aids in their identification. Compounds **36** and **40** displayed a major decomposition peak that did not exhibit the zinc isotopic pattern.

E. IR. Twenty-four of the most intense peaks within the range 4000−200 cm^{-1} for each compound are compiled in Table 13 of the Supporting Information. Because of discrepancies in the literature,[19,20] molecular modeling was employed to calculate the zinc−nitrogen stretch frequencies for the zinc bis(*tert*-butyl)(TMS) amide compound **27**. The calculated and observed spectra are shown in Figure 4 of the Supporting Information.

F. UV/vis. Observed λ maxima and the calculated molar absorptivities are shown in Table 14 of the Supporting Information for each zinc bis(amide) compound.

4. Elemental Composition. A. C/H Elemental Analysis. The purity of all zinc bis(amide) compounds was verified by determining their carbon and hydrogen content. The theoretical and the experimental values for these analyses are listed in Table 15 of the Supporting Information.

B. ICP. On the basis of a series of zinc dichloride standard solutions ranging from 0.0001 to 10 ppm, samples of zinc bis(amide) compounds of theoretical approximate zinc concentrations of 1 ppm were prepared, and the metal content was measured by ICP. Along with the theoretical values, the data are contained in Table 15 of the Supporting Information.

5. Thermal Properties. TGA. The initial onset temperature for mass loss, the temperature at which there is 50% weight loss (TGA_{50}), and the final temperature for mass loss for each of the zinc bis(amide) compounds are shown in Table 16 of the Supporting Information. If the final residual weight percent exceeded 10, the value is given parenthetically.

Discussion

Secondary Amines. Compilation and examination of data trends present within a series of compounds often provide insight into the selection criteria for utilization in a given application. The present study required a diverse set of ligands for precursor synthesis. When designing suitable precursors, ones possessing both high vapor pressure and vapor phase stability, ligand selection is one of the most important aspects of molecular design to consider. The ultimate goal of such an approach is the development of a protocol for converting searches from random "trial and error" to a logical scheme, one that targets a few select compounds. The starting point for this process, evaluation of ligand properties, is discussed first.

Upon examination of the ^{29}Si NMR spectra for the selected secondary amines (Table 3 of the Supporting Information), it is observed that signals for compounds **6**, **14**, and **21** (−2.62, −2.64, and −3.26 ppm, respectively), each of which has a quaternary α-carbon, tend to be shifted upfield, relative to those bearing a lesser degree of substitution at the α-C (0.48−7.21 ppm). Electron-donating (alkyl) groups increase the electron density around the nitrogen atoms, strengthening the electron overlap between the silicon and nitrogen linkage, thus leading to an increased shielding of the silicon atoms in these three compounds.

Mass spectra of amines are characterized by a β-elimination to initiate the cleavage cascade.[22] This characteristic is displayed by all investigated compounds, in conjunction with displaying loss of a radical species from the alkyl or silyl substituent, as illustrated in Scheme 4 of the Supporting Information [for HN(*n*-butyl)(TMS)]. Mindful of the electronegativities (N > C > Si), there are three possible eliminations for the *n*-butyl derivative **3** that result in an electron deficiency on either the silicon or the carbon atom. When the electron density is shifted toward the nitrogen−carbon bond, the weaker silicon−nitrogen bond can be cleaved, thus producing one neutral and one cationic silicon species. Additionally, the available proton on the nitrogen allows for elimination of methane via a four-membered intermediate. Another feature of the fragmentation pathways is explained by the loss of a neutral propene fragment via a six-membered intermediate. All the investigated amines demonstrated similar fragmentation patterns as described above.

A correlation in bond stability of ligand−hydrogen bonds with the corresponding metal−ligand interactions previously has been reported.[23] Thus, it was of interest to explore if this relationship was manifested in the present examples. In a comparison of the nitrogen−hydrogen stretching mode frequencies in the infrared spectra (Table 5 of the Supporting Information), the compounds that were shifted to lower values indicated lower energy processes and improved stability. The lowest energy hydrogen−nitrogen bond vibrations were observed for compounds **6**, **14**, and **15** (3383, 3383, and 3390 cm^{-1}, respectively). Two vibrations were observed for compounds **18** (3414 and 3329 cm^{-1}) and **21** (3415 and 3387 cm^{-1}) in the nitrogen−hydrogen stretch region, due to the presence of both free and hydrogen-bonded forms of the amines.[24]

(22) Pavia, D.; Lampman, G.; Kris, G., Jr. *Introduction to Spectroscopy: A Guide for Students of Organic Chemistry*; Saunders College Publishing: Orlando, FL, 1979; pp 272−276.
(23) Schock, L.; Seyam, A.; Sabat, M.; Marks, T. *Polyhedron* **1988**, *7*, 1517.
(24) Bellamy, L. *The Infrared Spectra of Complex Molecules*, 3rd ed.; Wiley: New York, 1975; Chapter 14.

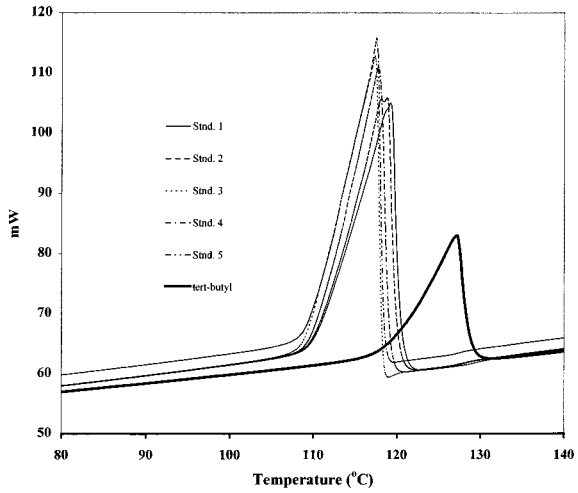

Figure 2. DSC data for toluene (standard) and HN[(*t*-Bu)(TMS)]$_2$, **6**.

The ultraviolet/visible spectra of all the examined compounds, except **15** (λ_{max} = 242 nm; for all other compounds, λ = 208−210 nm) and **19,** contain a single transition representing the promotion of the lone pair of nitrogen into the empty d orbitals of the silicon of allowed symmetry. Both exceptions contain aromatic rings, which result in an additional transition attributed to the nitrogen lone pair into empty π^* orbitals of carbon atoms constituting the ring. Also, the molar absorptivities for both compounds **15** and **19** are distinctly higher (ϵ = 7986 L mol^{-1} cm^{-1} for **19**; ϵ = 8691 L mol^{-1} cm^{-1} for **15**) than for the remaining amines (ϵ = 709−5256 L mol^{-1} cm^{-1}).

Determination of Boiling Points of Secondary Amines Using DSC. DSC was employed to determine the boiling points of all investigated compounds at atmospheric pressure. The leading edges of the peaks, shown in Figure 2, represent the section of the experiment where the sample temperature was constant at the boiling point while the calorimeter temperature was increasing at the specified heating rate. The isothermal boiling condition is achieved only when the entire volume above the sample is occupied by its vapor.[25] To accomplish this, a 50 μm laser-drilled hole in the sample lid serves to ventilate the sample, allowing other gaseous materials to exit during the onset of the boil-off. The aperture also prevents pressure buildup, which would result in the sample container's rupture.[26] Precautions were taken to ensure that each analyte had the same volume and initial equilibration time for comparison purposes. The exact boiling point was determined by calculating the onset of the endothermic event. The height and area of the peak are dependent on the volume and volatility of the sample. Four standard samples were analyzed five times each and the results averaged to determine the precision and accuracy of the technique. In addition, three separate onset calculations of each endothermic event were averaged. The results are listed, showing standard literature values and percent error: toluene, 110.6 °C, 109.5 °C, 1.1%; cumene, 153.0 °C, 152.4 °C, 0.6%; analine, 184.4 °C, 184.5 °C, 0.1%; dicyclohexylamine, 256.0 °C, 256.2 °C, 0.08%. The reported value for cumene was 152−154 °C; consequently, the average was used in the error calculations.

Zinc Bis(amide) Compounds. All synthesized zinc bis[(alkyl)(trimethylsilyl)amide] derivatives were either colorless viscous liquids or colorless crystalline solids. The products were extremely sensitive to oxygen and moisture. Table 8 of the Supporting Information summarizes the boiling points of the HN(R)(TMS) compounds acquired by DSC (as described previously). A comparison of the TGA data for the zinc bis(amide) compounds (Figure 3) indicates the *i*-propyl derivative to be the most volatile compound of the present study, at 1 atm. Although the precise ranking of the six lowest boiling secondary amines, and their derived amides, does not track, the trend of the grouping of the lowest boiling point amines translates to the grouping of the most volatile amides. There are two notable exceptions to this trend, the *n*-propyl and *n*-butyl derivatives (compounds **22** and **24**, respectively), each of which exhibited reduced volatility, which presumably is a consequence of residing as ambient temperature dimers.

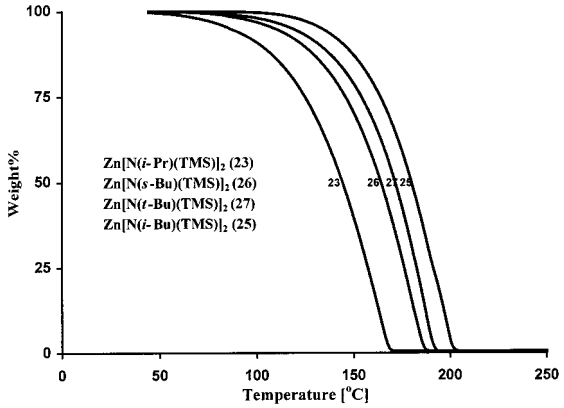

Figure 3. TGA data for selected Zn[N(R)(TMS)]$_2$ compounds (R = *i*-Pr (**23**), *s*-Bu (**26**), *t*-Bu (**27**), *i*-Bu (**25**)).

Two dynamic ligand-binding processes may be invoked to explain the observation of multiple peaks in the ^{1}H and ^{13}C spectra for **22**, **24**, **29**, **30**, **38**, and **41** (Tables 9 and 10 of the Supporting Information). The presence of both terminal and bridging ligands in the dimeric form partially explains the multiple signals seen at ambient temperature (**22** (*n*-Pr): ^{1}H NMR, multiplets at 3.13 and 2.79, triplets at 0.92 and 0.80, singlets at 0.30 and 0.26 ppm; ^{13}C NMR, 51.54/50.83, 33.08/32.63, 11.67/11.41, and 2.92/2.01 ppm). Elevated-temperature experiments demonstrate that both signals become equivalent on the NMR time scale. This reversible event is illustrated in Figure 5 of the Supporting Information, where the ^{1}H signal from the methyl substituents on the silicon is observed at various temperatures for compound **22** dissolved in deuterated toluene. There are two possible isomers, including the bridging substituents on nitrogen in a cis or trans configuration, with respect to the TMS groups. The trans arrangement is energetically favored to minimize the steric hindrance of the large silyl substituents. This additional smaller peak coalesces prior to heating to ambient temperature. The two main peaks spread apart as the temperature is increased and then broaden into coalescence. Subsequently, a single peak is resolved at a position of greater shielding, compared to the initial shifts, at 245 K. Thus, the NMR data cannot be interpreted solely by a two-site exchange mechanism, but instead by the existence of multiple dynamic processes. Comparable behavior was witnessed for compounds **24**, **29**, **30**, **38**, and **41**; however, the coalescence temperatures rose as the molecular weight increased.

In contrast to the behavior displayed by the ^{1}H NMR data, the observed multiple peaks in the ^{29}Si spectra (Table 11 of the Supporting Information) did not coalesce with increasing temperature (**22** (*n*-Pr): 9.71 and 0.73 ppm); rather, the two signals broadened (8.59 and 0.41 ppm) substantially (~160 Hz at half-height). This could be attributed to incomplete dissocia-

(25) Perkin-Elmer. *Determining Vapor Pressure by Pressure DSC*; Thermal Analysis Newsletter (PETAN-49).

(26) Brozena, A.; Cassel, R.; Schaumann, C.; Seyler, R. *Vapor Pressure Determination using DSC*, 22nd Conference of the North American Thermal Analysis Society Proceedings, 1993.

tion of the dimeric species. If there were a single equilibrium process, then the ^{29}Si signals would have merged at temperatures corresponding to the ^{1}H data, and the three regions of compounds **24**, **29**, and **30** would have simultaneously coalesced. The cleavage of the dimer does not necessarily occur in a concerted fashion; an intermediate consisting of a single dative bond allows for rotation, which results in broadening of the signals, as observed for the ^{29}Si data.

The chiral ligands **5**, **10**, **11**, and **13** possess the potential of forming three different isomeric forms of the corresponding zinc bis(amide) compounds. The ligand conformations can be classified into two groups where the chirality of the two amine substituents either are similar (meso) or are opposing (D or L), leading to multiple signals for select peaks in the ^{1}H and ^{13}C spectra (e.g., compound **26** derived from ligand **5** displays the following signals in the ^{13}C NMR spectrum: 53.04, 39.86, 39.79, 31.45, 31.33, 11.73, and 2.39).

The spectra of compounds **36** (R = phenyl) and **40** (R = benzyl) also displayed multiple peaks; however, the pattern was unlike those of the previous cases. The ^{1}H and ^{13}C spectra were a mixture of sharp and broad peaks. Acquiring spectra at an elevated temperature merged the peaks into broad singlets (^{13}C NMR: **36**, 129.64, 126.92, 123.61, 120.04, 2.42; **40**, 148.29, 129.48, 128.15, 127.32, 51.19, 1.27; width different for each nucleus) that corresponded well with expected results. Additional bonding modes associated with the aromatic rings in conjunction with the bridging and terminal differences described earlier combine to create the complex spectra observed at ambient temperature. In these examples, the peaks of the ^{29}Si spectra coalesce at elevated temperature, unlike the derivatives discussed above.

To acquire mass spectra, samples were filled in an inert atmosphere and flame-sealed in melting point capillaries at atmospheric pressure. When the tube was broken, sufficient headspace was present to prevent atmospheric penetration to the compound during direct insertion into the spectrometer sample orifice. In the mass spectral data, the characteristic isotopic pattern for zinc was observed in both the molecular ion and other smaller zinc-containing fragments for all the zinc bis(amide) compounds examined in this study. A network of potential pathways is presented in Scheme 5 of the Supporting Information for Zn[N(*tert*-butyl)(TMS)]$_2$ (**27**). The fragmentation pattern follows a route similar to that of its ligand, in which the initial steps involve β-eliminations of radical species. There exist three possibilities, and each of the resultant fragments was observed. With the aid of MS/MS techniques, the rest of the pathways were constructed. When the electron density is localized about the nitrogen−carbon bond, both the zinc−nitrogen and silicon−nitrogen interactions are weakened, which can enhance the cleavage. The remaining routes are characterized by fragment loss with a hydride shift. The smallest observed zinc-containing fragment has a molecular mass of 138 amu with a feasible molecular formula of C_2H_8NSiZn, thus supporting the possibility of retaining the valuable zinc−nitrogen linkage.

The mass spectrum for compound **27** indicates a molecular mass of 243 amu, which does not have the characteristic isotope pattern for zinc. Scheme 3 illustrates two potential mechanisms to explain the observed peaks of 243 and 114 amu. From the MS/MS data, the 234 amu peak was observed to be a daughter of fragment 337. Other MS/MS experiments suggested the peak likely results from a mechanism involving a species yielded from the β-elimination of a substituent on silicon. The proposed mechanistic pathway begins with a shift of the unfragmented ligand to the silicon, thus moving the positive charge to the

Scheme 3. Proposed Fragmentation Pathways for Zn[N(*tert*-butyl)(TMS)]$_2$ (**27**)

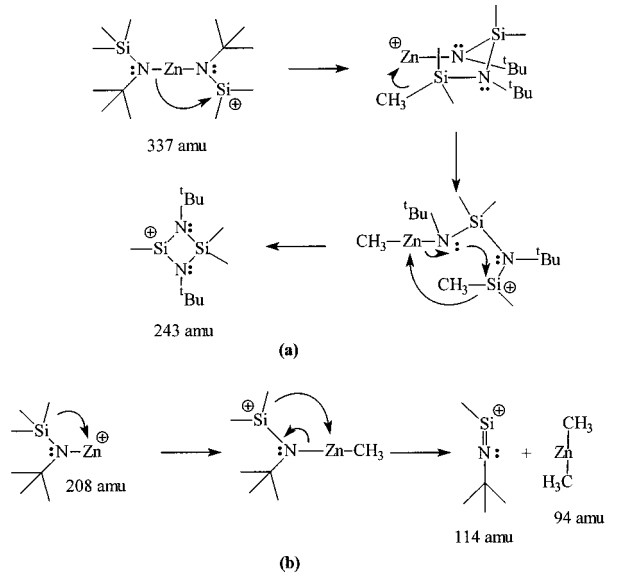

zinc. After a methyl shift to the zinc, via a six-membered transition state, a nitrogen−silicon ring closure is consummated. Another methyl shift to the zinc precedes the elimination of dimethylzinc, thus leaving the positively charged 243 amu fragment. Potentially, two methyl shifts to the zinc (from the proposed structure for peak 208) followed by elimination of dimethylzinc would explain the 114 amu fragment. Raston et al. noticed analogous behavior for a corresponding cadmium bis(amide) system.[27] The molecular ions for compounds **22**, **24**, **29**, **30**, **36**, **38**, **40**, and **41** each indicate monomeric structures in the gas phase.

IR samples for the moisture-sensitive compounds were prepared inside an inert atmosphere glovebox and sealed inside a plastic bag filled with argon. The minimal time the sample holder was exposed to the atmosphere during transfer from the argon bag to the spectrophotometer only permitted decomposition of the outer edges of the compound, between the salt plates, while the center scanning area remained unchanged. The infrared spectra feature no evidence for N−H stretches found in the amine IR spectra (3383−3415 cm^{-1}), indicating successful conversion of the secondary amine to the corresponding amide.

Difficulty in determining the frequency for the zinc−nitrogen symmetric IR stretch led to a molecular modeling approach to computationally predict the spectrum of **27**. The structure was optimized multiple times with increasing levels of theory to ultimately shorten the processor time required. The molecule was constructed to resemble the solid state structure[11] with the N−Zn−N angle set at 180° and the resulting dihedral angle formed by the Si−N−N−Si arrangement set at 90°. The structure was first optimized using an ESFF force field in the Discover module followed by minimizing the energy using the AM1 Hamiltonian in the MOPAC module. Finally, four optimizations utilizing the Hartree−Fock method in the Turbomole module were conducted with sequential increasing basis set size (STO-3g, 3-21g, 6-31g, and 6-31g**). The frequency calculation was performed employing the 6-31g** basis set. Upon completion, the calculated spectrum provided a good fit to the observed data (Figure 4 of the Supporting Information). Within the BIOSYM software, the constituent molecular vibra-

(27) Englehardt, L.; Junk, P.; Patalinghug, W.; Sue, R.; Raston, C.; Skelton, B.; White, A. *J. Chem. Soc., Chem. Commun.* **1991**, 930.

tions associated with each frequency can be animated to aid in interpreting the IR spectrum.

On the basis of the above prediction, the region from 900 to 325 cm^{-1} consists of peaks with asymmetric Zn−N stretch contribution, while the domain from 325 to 200 cm^{-1} involves a symmetric Zn−N stretch component. This relates to compounds **23**, **25**, **26**, **28**, **31**, **33**−**35**, **37**, and **42**, which are presumed to reside as monomers at ambient temperature on the basis of the previously discussed NMR data. As a consequence of the complex nature of the fingerprint region, it is difficult to select a particular Zn−N vibration for a refined comparison without further calculations, which require extensive computer time. Focusing on the region 460−400 cm^{-1} for comparison of the zinc bis(amide) compounds, Figure 4 of the Supporting Information depicts the similarity between the selected Zn−N vibration region and the N−H stretch for the corresponding amine ligands. Compounds **22**, **24**, **25**, **27**, **30**, **36**, and **39** are each solids at ambient temperature; thus the spectra were obtained via a Nujol mull, while all liquids were collected in neat form.

UV/vis samples also were prepared inside an inert atmosphere glovebox. The Teflon cap of the quartz cell was sealed adequately and was aided by the positive vapor pressure of the utilized solvent (THF) to minimize atmospheric contamination during the scanning process. An additional broad shoulder (250−300 nm), relative to the corresponding data for the secondary amine, appeared in the UV/vis spectra of the zinc bis(amide) compounds, which corresponded to the transition of the electron density of the nitrogen into the empty orbitals of the metal.

The TGA of each zinc bis[(alkyl)(trimethylsilyl)amide] compound, obtained on an instrument inside an inert atmosphere glovebox, showed that all precursors vaporized in one step with minimal decomposition. The most volatile representative, according to the TGA data, is $Zn[N(i\text{-propyl})(TMS)]_2$ (**23**), as depicted in Figure 3. The least volatile species were the compounds containing straight-chained alkyl substituents, such as *n*-propyl or *n*-butyl (Table 16 of the Supporting Information). This correlates with the fact that these species are believed to be dimers at ambient temperature. However, there is not a large difference observed between the dimers and monomers, as would be expected if based solely on molecular weight. This is explained by dimer cleavage prior to phase change. The vaporization of a monomer versus a dimer requires less energy; consequently, the volatility would be influenced by the energy needed to cleave the dimer. In addition, it is this separation of the moieties that exposes the zinc−nitrogen linkage to a nucleophilic attack; subsequently, this can lead to decomposition. Therefore, the bulkiness of an alkyl group, or more precisely, the nature of the substitution of the carbon α to nitrogen, is of importance to the kinetic stability of the compounds.

Conclusions

An extensive investigation of a series of zinc bis[(alkyl)(trimethylsilyl)amide] compounds has been conducted, employing both conventional, as well as several new, secondary amines in the role of amide precursors. Noteworthy among the data is the emergence of a wide range of vapor pressures for examples of this class of organometallic compounds. One of the more volatile compounds examined in this exploration, $Zn[N(i\text{-propyl})(TMS)]_2$, **23**, has been subjected to additional study[28] as a potential dopant source compound for organometallic vapor-phase epitaxy (OMVPE) of ZnSe:N.[29] Additionally, a new technique has been described for boiling point determination of milligram-size samples. These, and other related results, will be the topics of upcoming publications.

Acknowledgment. The support of the Office of Naval Research and the Georgia Institute of Technology Molecular Design Institute for this work is gratefully acknowledged. W.S.R. was the recipient of an Alexander von Humboldt Award with Prof. Dr. H. Schumann at the Technische Universität Berlin (1998−1999).

Supporting Information Available: Tables 1−16 listing NMR, EI-MS, IR, UV/vis, elemental analysis and yield data, alkyl subsituent identities, preparation methods, and boiling points for (R)(TMS)NH and $Zn[N(R)(TMS)]_2$ compounds, Schemes 4 and 5 depicting fragmentation pathways for **3** and **27**, and Figures 4 and 5 depicting IR spectra for **27** and NMR data for **22**, respectively. This material is available free of charge via the Internet at http://pubs.acs.org.

IC000234J

(28) Rees, W. S., Jr.; Gaul, D.; Just, O.; Heuken, M.; Taudt, W. Unpublished results.
(29) Rees, W. S., Jr. In *CVD of Non-Metals*; Rees, W., Jr., Ed.; VCH: New York, 1996; pp 1−35.